Prediction of microgeometrical influences on micropitting fatigue damage on 32CrMoV13 steel

A. Fabre [a,*], H.P. Evans [b], L. Barrallier [a], K.J. Sharif [b], M. Desvignes [a]

[a] Arts et Métiers ParisTech, MécaSurf Laboratory, 2, Cours des Arts et Métiers, 13617 Aix-en-Provence, France
[b] Cardiff School of Engineering, The Parade, Newport Road, Cardiff CF24 3AA, UK

A B S T R A C T

Micropitting is a form of surface fatigue damage that occurs in the gear teeth. It is due to the effect of variation in the mechanical loading in the contact zone between the two teeth, induced especially by flank roughness. In this study, generic roughness profiles were built with geometrical parameters to simulate the contact between two rough surfaces. Using elastohydrodynamic lubrication code and Crossland's fatigue criteria, the influence on fatigue lifetime was analysed for changes in each parameter. The relevant parameters were determined that influence (i) the conventional pitting, (ii) the extent to which the von Mises equivalent stress exceeds the material yield stress in the zone where micropitting occurs, and (iii) the fatigue lifetime for steel teeth. With nitriding benefits, the same trends were shown with weaker effects.

Keywords:
Micropitting
Fatigue damage
Microgeometry
Gear

1. Introduction

Micropitting is a form of fatigue damage. It occurs in the contact zone of a mechanism where changes in mechanical loading on the surfaces of the two bodies are induced [1,2]. It is a form of failure in gear contacts and has characteristic pitting of the surfaces at the scale of the surface roughness features. These pits can grow and through crack branching can eventually lead to tooth breakage. In gears, it was demonstrated [3–5] that the location of this damage is close to the surface near the root of the teeth and occurs where the slide/roll ratio ξ is higher [6].

A global analysis of the causes of micropitting can be separated into three different factors, the boundary conditions, the change of the surface under load at the operation conditions, and the capability of material to resist the mechanical loading. The first factor is directly linked to the boundary conditions in the contact zone when meshing of teeth occurs, which are generally subject to elastohydrodynamic lubrication (EHL) or mixed EHL/boundary lubrication conditions. Some studies have been conducted to examine the lubricant effect on the micropitting features. These experimental analyses investigated the influence of additives on the thermo-physical properties [7]. The boundary conditions in the contact zone are mainly dependant on the thermo-physical and mechanical properties of lubrication, and on the interaction between the roughness and the lubricant film [8].

The second factor is due to the response of the material in the contact zone to the mechanical loading during the few first cycles of operating system. Some rolling experimental studies [9,10] investigated this effect in terms of microgeometry changes due to the scission of some asperities and plastic strain phenomenon on asperities. Some modelling has been carried out to analyse this effect in the case of sliding and rolling contact [11]. Nevertheless, no study has treated the full effect of running-in taking into account the changes in material behaviour, the cumulated damage, and at the same time the changes of geometry.

The third factor is the response of the material in terms of limited fatigue or infinite lifetime. Because the fatigue lifetime depends on the mechanical properties of the material in terms of resistance to failure under variable transient loading, some studies have been conducted based on the analysis of real roughness profiles [6] under EHL conditions where the influence of the slide/roll ratio was demonstrated. In other studies, predictions of behaviour were developed taking into account the pressure distributions attributable to sinusoidal roughness [12,13]. However, in all these analyses the mechanical loading was the applied loading but the residual stresses induced by the machining process was not taken into account.

The originality of the current study is in the generation of roughness profiles in order to produce a parametric study of predicted micropitting behaviour. In the contact zone, damage can occur due to wear or to fatigue mechanisms. The work is focused on determination of the fatigue damage that occurs in the first 50 micrometres beneath the surface. This study deals with a simulation of the effect of EHL loading on the contact zone taking actual

* Corresponding author. Tel.: +33 442938198.
E-mail address: agnes.fabre@ensam.eu (A. Fabre).

http://dx.doi.org/10.1016/j.triboint.2012.07.018

conditions and materials into account. In this approach, the semi-analytical modelling of the history of loading is treated for the case of elastic strain. Moreover, in the case of nitriding, residual stresses are introduced in the global loading taking the changes due to deep gradient of properties into the calculation. Because of the small size of the micropits, general plasticity is not occurring in the contact zone during the micropitting process. This form of damage can occur locally after several cycles of loading corresponding to tooth meshing (when the teeth are in contact) due to a local plasticity of grains of material. However, it is not possible to know precisely the arrangement of the microstructure and to determine the position and the orientation of the local grains directly linked with the position of the specific asperities close to the surface for this study which is based on parameterised roughness profiles without consideration of sub asperity grain structures. The approach developed in this work could not use specific microscopic fatigue criteria without any information or knowledge of position and orientation of grains, slip planes and local defects of the material. Such features would be more appropriate for study of real measured surface profiles where metallurgical examination of the grain structure is possible. For the current study mechanical calculations are conducted considering small volumes based on the assumption of a homogeneous and isotropic material. The Crossland criterion [14] is used to predict fatigue and was developed to consider the effects of large hydrostatic pressures on fatigue which is a feature of the loading experienced by the asperities. It is based on two invariants of the stress tensor. The first factor is the alternate von Mises stress, in order to take into account the changes in time in the mechanical loading that induces local plasticity, and the second is the maximal hydrostatic pressure. This is a multiaxial fatigue criterion, based on a macroscopic approach to damage, taking into account the capability of the material to resist to the failure. Failure of a material is defined when the damage parameter is equal to 1. Because this phenomenon can occur after a long service time for gears, the assumption of linear accumulation of damage can be made and is consistent with the elasticity loading hypothesis. With these hypotheses, fatigue lifetime was quantified and the most relevant parameters of the roughness profiles were identified.

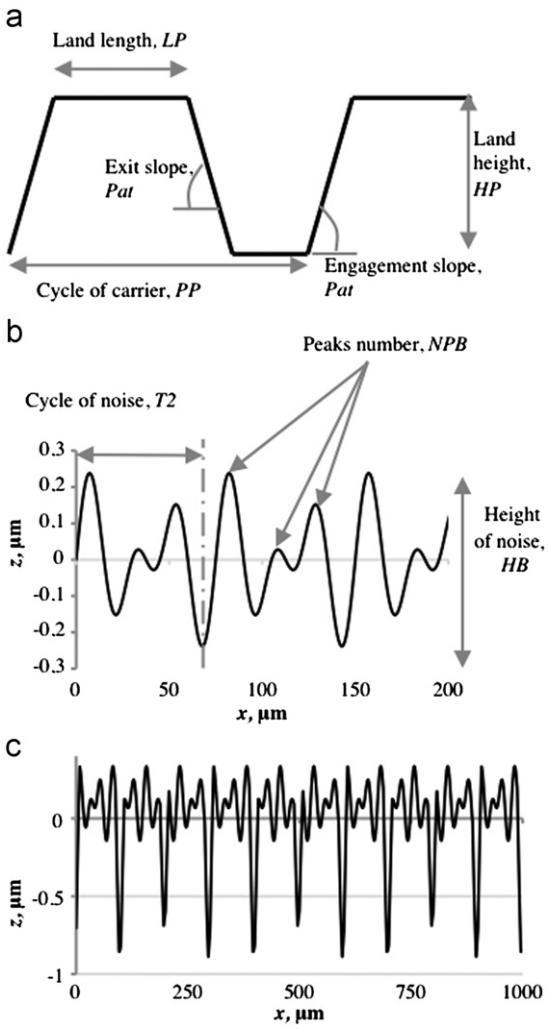

Fig. 1. (a) Carrier component, (b) noise component, (c) resulting profile.

2. Hypothesis and method

2.1. Geometry

The roughness of the pinion and the wheel contacting surfaces are defined using generic profiles specified in terms of a set of parameters. The goal is to be able to represent the real micro-geometry of the surfaces obtained on ground, or superfinished gear teeth. In order to reproduce the typical large bearing area of this finished surface, the profile is built on a carrier specified with four parameters illustrated in Fig. 1(a): HP, the height of the carrier; LP, the length of the carrier land; PP, the total length or the carrier cycle; and Pat, the (equal) engagement and exit slopes. This work is aimed at examining surfaces finished by an abrasive machining process. The surface then presents a specific geometry with broken grains or sheared grains on the boundaries. In order to take the geometry induced by the grains of material into account, a noise defined by three parameters illustrated in Fig. 1(b), is added to the previous carrier. The noise parameters are: HB, the height of the noise; T2, the period of the noise; and NBP, the numbers of peaks. An example of the resulting generated profile is shown in Fig. 1(c). Analysis of the microstructure of the material has led to choice of a minimal periodicity of the noise consistent with the grain size of over 10 µm. However a spatial resolution of at least a set of 3 grains is considered necessary to be sufficient for effective calculations using the hypothesis of isotropic and homogeneous material in the EHL simulations. Real profiles of roughness were analysed and the results of examination allowed the minimal, and maximal values for all the other profile parameters involved in the study to be defined. Fig. 2 shows an example of a real rough profile with different values of local measurements of height and length. A mean profile was defined using the mean profile values specified in Table 1. In order to investigate the effect of parameter variations about forty profiles were generated for the study. Each of these profiles had a variation in one of the seven parameters with the others taking the mean profile values. Table 1 also gives the minimal and maximal values used for each parameter's variation.

For all these profiles the values of the standard roughness parameters are very close to the range of those obtained for real ground or superfinished surfaces [15]. The extreme values of the arithmetic roughness, Ra, the skewness, Rsk, and the kurtosis, Rku, obtained for the profiles considered are given in Table 2, [16].

2.2. Materials

2.2.1. Base material

The material used as a basis for this study for the wheel and the pinion is the 32CrMoV13 steel grade quenched and tempered in order to obtain a yield point of about 1 GPa (tempered martensite). The grain size is about 10 µm and the chemical composition is given in Table 3. Residual stresses of the base

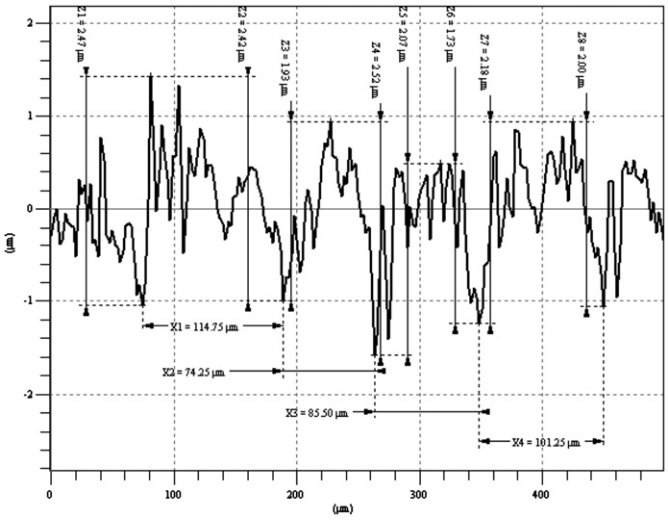

Fig. 2. Example of a real roughness profile.

Table 1
Mean profile parameter values and Minimal & Maximal parameter values used for the generic profiles.

Designation	Mean profile value	Minimal value	Maximal value
HP, land height, µm	0.8	0.3	3
LP, land length, µm	80	40	90
PP, cycle of carrier, µm	100	89	160
Pat, exit or engagement slope	0.1	0.1	1
HB, height of noise, µm	0.5	0.1	1
T2, period of noise, µm	30	30	90
NPB, peaks number	3	1	5

Table 2
Limits of the roughness parameters for the generic profiles used in the study.

Standard roughness parameters	Minimal value	Mean Profile	Maximal value
Ra, arithmetic roughness, µm	0.1	0.2	0.7
Rsk, skewness, µm	−2.2	−1.6	−0.2
Rku, kurtosis, µm	1.4	5.2	8.4

Table 3
Chemical composition of the 32CrMoV13 steel (in wt%).

Material	C	Si	Mn	Cr	Ni	Mo	V	Fe
	0.305	0.33	0.47	2.92	0.14	0.87	0.30	Balance

material are neglected because of their low values and because no significant changes in these values can be detected with depth.

2.2.2. Nitrided material

With thermo-chemical treatment such as gaseous nitriding this grade of steel can be modified by the precipitation of alloyed nitrides beneath the surface to a depth of about 1 mm [17]. Due to the nitriding, changes occur in the microstructure that induce mechanical benefits of two kinds. First there is an increase in the hardness value and also in the yield strength of the material close to the surface [18], and the fatigue lifetime [19] is increased as a result of these changes due to nitriding. The second effect is generation of compressive residual stresses beneath the surface [20,21]. This induces a new mechanical loading to be added to the surface loading applied to the part in the contact zone which can also have beneficial consequences.

In the current study analyses are conducted for the standard base material and also for the material when it has been nitrided. Comparison of these results allows the effect of nitriding to be assessed. The changes of yield strength and residual stresses with depth beneath the surface were specified using formulae fitted to experimental data obtained in previous work at the MécaSurf Laboratory [22,23]. Because of the brittle nature of the white layer essentially constituted with iron nitrides, due to the grinding operation, a removal of about 100 µm of the surface material was assumed. Changes in yielding point were taken a value of 2 GPa at the surface of the parts. The residual stresses were assumed to be biaxial taking the geometry of the tooth into account with a large radius of relative curvature of about 38 mm in the contact zone far from the fillet [24,25] in the specific case of the straight spur gears studied. As shown in Table 4, the Young's modulus and Poisson's ratio were assumed to be the same with and without treatment, disregarding the weak effects of nitriding on these mechanical properties of the steel.

2.3. Mechanical effects

2.3.1. Surface loading

The study deals with a pinion and wheel under realistic operating conditions focusing on the main damage zone. Surface loading is obtained using simulation under fixed conditions in terms of radius of curvature, slide-roll ratio, contact load and velocity. The different values of load and velocity assumed in the analyses are given in Table 4. The properties of OEP-89 oil grade were used in calculations as this naval gear oil is the test oil used in a test program associated with this work. The specification includes non-Newtonian behaviour of the oil as this is a relevant factor in determining surface shear loading in sliding contacts [26]. The relative radius of curvature corresponds to that of the gear pair considered when contact occurs at the specified slide-roll ratio, ξ. The surface studied corresponds to the pinion, which is the slower moving surface relative to the contact point as discussed in Section 2.3.2. The value of ξ was chosen taking into account the geometry of the gear and the location where micro-pitting was first observed in experimental analysis [2,5].

The current study deals with spur gears and the investigation was carried out with a two-dimensional transient line contact approach. In the contact zone, the surface loading was calculated using a transient line contact elastohydrodynamic (EHL) code that takes into account the roughness of the pinion and the wheel. The EHL code is based on fully coupled and simultaneous solution of

Table 4
Operating conditions of the gear simulated used for EHL calculations and mechanical and physical properties for steel and oil.

Operating conditions	Radius of relative curvature, mm	38,1
	Line contact loading (L), kN/m	387.1
	Relative velocity between the teeth (S), m/s	5.8
	Slide/roll Ratio ξ	0.655
Mechanical and physical Properties	Young's Modulus (E), GPa	206.9
	Poisson' ratio (ν)	0.3
	Yielding point, 32CrMoV13 quenched & tempered, MPa	1000
	Yielding point, 32CrMoV13 nitrided on the surface, MPa	2000
	Viscosity at ambient pressure (η), Pa s	0.0842
	Viscosity pressure coefficient, GPa^{-1}	13.5
	Eyring shear stress, MPa	10

Reynolds equation and elastic deflection of the contacting bodies [27–30]. The output data corresponds to the surface loading given at different time steps within the transient analysis in terms of normal loading, $p(x,t)$, and tangential loading, $q(x,t)$. The time step for the analysis is specified such that the positional change per timestep for the faster moving surface is ½ the spatial mesh spacing for the EHL analysis [29,30]. The loading is given for all the meshing points defined in the window of the contact zone studied, i.e. the EHL solution space which is fixed relative to the contact point. The assumed input data are given in Table 5. These values were chosen in agreement with the optimal timestep magnitude established by Holmes et al. to produce optimal and consistent solutions to the transient micro-EHL problem [31]. In the current study, the EHL calculations have been conducted for contact between two rough surfaces having the same roughness profile. The results are compared with the results obtained in a previous study dealing with smooth on rough surfaces [32].

Table 5
Input data for EHL calculations.

Designation	value	unit
a, half contact width	235	μm
Window width (solution space)	−2.5a to 1.5a	μm
Spatial mesh spacing	1.18	μm
Time step advance of the slow surface	0.30	μm
Time step advance of the fast surface	0.59	μm
Number of timesteps	15,000	timesteps
Storage of the data	Every 10	timesteps
Length of rough profile	10	mm
Step for roughness profile definition	0.25	μm

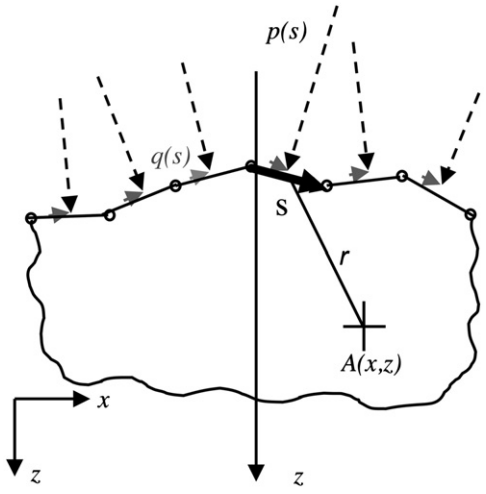

Fig. 3. Surface loadings contribution on the stress tensor on the point A, with lateral position x and in-depth position z.

2.3.2. Sub-surface stress

Sub surface loading was calculated in a fatigue analysis software tool developed using the C++ language. This calculates the stress component values for each sub-surface point considered as illustrated in Fig. 3 using the method described in [32,33] assuming elastic plane-strain conditions. For each timestep of the EHL calculation, as shown in Fig. 3, the normal loading $p(s)$ and tangential loading $q(s)$ are given as boundary conditions on the rough deflected surface leading to the stress tensor at points beneath the surface such as $A(x,z)$.

With the hypothesis of an elastic half-space, the mechanical effects of all these loadings are summed by superposition using an analytical approach [34]. With this second stage of calculation, the history of stress components is obtained in the coordinate system fixed in the pinion for each point $A(x,z)$. Typical variation in the stress components with time are given for the same point beneath the rough surfaces in Fig. 4 which compare the case where the point considered is part of the slower moving surface with the case where it is part of the faster moving surface. This comparison shows that the slower moving surface is subject to more stress variation, in terms of oscillations, during its passage through the contact zone and it is the focus of the current study on analysis of stress history and fatigue life. The conditions thus correspond to those of the area of a pinion tooth where meshing first occurs which is the area where micropitting occurs in gear contacts.

The stress tensor was determined for different material points beneath the surface. The material volume considered was 1.5 mm long and the stress was determined at points separated by a lateral step of 10 μm. This value was chosen in order to conduct an analysis in agreement with the grain size of the material which is of the order of 10 μm. Perpendicular to the surface the meshing step was equal to 1 μm for the near-surface material with coarser resolution away from the surface according to the results obtained in each case. The fineness of mesh was continued to the depth of the last point where the value of equivalent von Mises stress, σ_{eqvM} was found to exceed the yield stress, σ_y. For cases based on non-nitrided material a larger meshing step of 10 μm, was taken for material from the position of the last point with $\sigma_{eqvM} > \sigma_y$ to a depth of 200 μm. This value was chosen in accordance with the position of the Hertz point, i.e. the point with maximum σ_{eqvM} in the case of smooth contact with normal

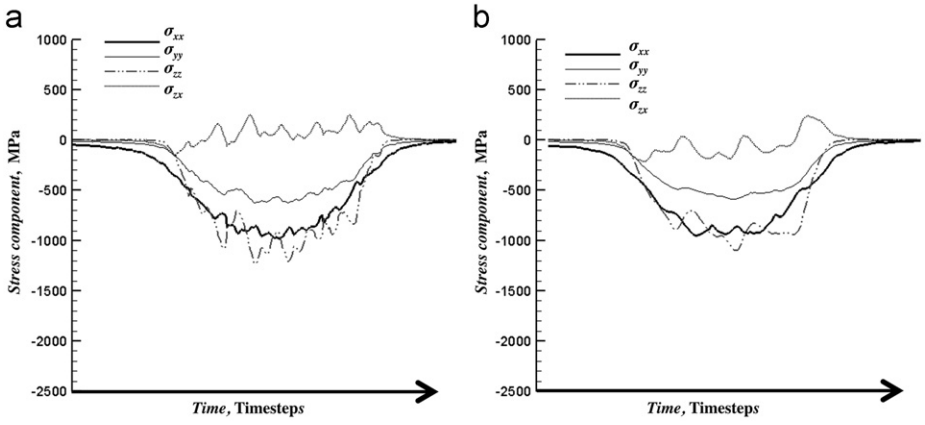

Fig. 4. Stress history for (a) the slow surface, and (b) the fast surface at the point with lateral position $x=3000$ μm and depth at $z=20$ μm beneath the surface.

loading expected to be at a depth of approximately 180 μm for the load case considered.

2.3.3. Equivalent stress evaluations

For the stress histories obtained for all the points in the material considered, the results were evaluated according to three criteria. The first was based on the maximal value of σ_{eqvM} obtained in the vicinity of the location of the maximum σ_{eqvM} for the equivalent Hertzian contact. The maximum was found in terms of all space positions in the material with depth greater than 100 μm from the surface for all the time values considered. All the points with $\sigma_{eqvM} > \sigma_y$ were closer to the surface and therefore eliminated in this analysis. This criterion allows finding the equivalent Hertz point, where pitting can occur. With this criterion, the influence of the profile parameter on pitting can be detected.

The second criterion was defined as the count of the number of points within the material with $\sigma_{eqvM} > \sigma_y$ during the time history. The value of this criterion is of interest as it gives a measure of the influence of the profile parameters on the severity of the loading. It also identifies the points $\sigma_{eqvM} > \sigma_y$ which are excluded from the fatigue analysis that is the third criterion. These points are excluded in order to be consistent with the assumption of elastic loading that is embedded in the fatigue lifetime analysis carried out as described in Section 2.3.4.

2.3.4. Fatigue analysis

Fatigue analysis was conducted using the Crossland criterion [14]. This hypothesis is based on invariants of the stress tensor and is relatively straightforward to apply to the case of gears for the screening purposes of the current study. The Crossland approach allows conditions for infinite life to be established and also allows finite life calculations to be carried out provided the loading remains elastic [35]. It is unsophisticated in comparison with critical plane models such as the Dang Van model [36] for example but is a solid basis to highlight the needs in terms of screening and future evaluation developments for this multiaxial fatigue study. During the meshing cycle all the stress components are simplified and assumed to have a sinusoidal cycle of loading. For each component, the mean stress, σ_m, and the amplitude σ^{alt}, are then sufficient to quantify the changes in the stress component history. The amplitude is defined as half the difference between the maximum and minimum values of the stress component. However as illustrated in Fig. 5, the shear stress may be out-of-phase with all the three normal components and this warrants special attention when changes in the history of stress components are to be analysed [37–39]. Fig. 6 shows the changes in σ_{eqvM} during the meshing. The out-of-phase phenomenon induces more than one local maximum. In this case of non-proportional loading, mechanical loading is assumed to be the sum of two separate loadings. The normal loading and the shear loading, each of these loadings induces damage during the meshing of teeth.

The cumulative damage, D is defined in order to take out of phase loading into account. With the hypothesis of a cumulative linear damage such as defined by Miner [40], the value of this damage for each cycle of loading is equal to N^{-1} where N is the number of cycles to failure. Then, with the hypothesis that failure occurs when D is equal to unity [35], D can be calculated by summing the different damage contributions in order to take into account the maximal changes for stress components that do not occur simultaneously. Equivalent damages D_{eq1} and D_{eq2} are defined such as that damage D_{eq1} is induced by the normal loading and the damage D_{eq2} is induced by the shear stress loading. With the linear cumulative hypothesis, these damages D_{eq1}, D_{eq2} are equal to ${N_{eq1}}^{-1}$ and ${N_{eq2}}^{-1}$ respectively for each

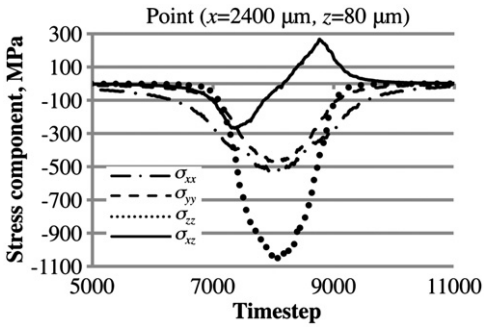

Fig. 5. Stress component history for a point beneath the surface.

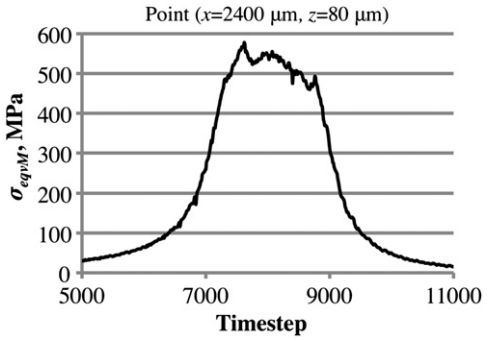

Fig. 6. Stress equivalent von Mises history for a point beneath the surface.

cycle of loading. The values of N_{eq1},N_{eq2} are the numbers of cycles to failure for the normal loading alone and the shear stress loading alone, respectively.

In the Crossland method, for each material point, the stress history is reduced to two items: the maximal hydrostatic pressure, Ph_{Max}, and the maximum of the equivalent alternate von Mises stress, σ^{alt}_{eqvM}. The definition of equivalent alternate von Mises stress is the value associated with the alternating stress tensor consisting of half the difference between each maximal and minimal component of stress in time. The Crossland diagram plots these variables against each other so that the position of the loading point, M, is given by the coordinates (Ph_{Max},σ^{alt}_{eqvM}) in the Crossland diagram.

By fitting at least two experimental Wölher fatigue curves with a Palmgren model [41], the capability of material can be described in the Crossland diagram as the straight line following Eq. (1). The Wölher fatigue curves with different stress ratios are useful in a specific domain in terms of numbers of cycles to failure. This domain is limited by the minimum and maximum numbers of cycles when failure occurred in the experimental characterisation of the material. Shown in Figs. 7(a) and (b), coefficients $\alpha(N)$ and $\beta(N)$ are the two characteristic parameters of the material for the number of cycles N to failure, with an associated risk of 50%. For a loading point M (Ph_{Max}, σ^{alt}_{eqvM}), if the Eq. (1) is true, then the failure occurs with a probability of 50%. If σ^{alt}_{eqvM} is larger than $\alpha(N) \times Ph_{Max} + \beta(N)$, then the failure will occur (with 50% probability) in less than N cycles. Likewise, if σ^{alt}_{eqvM} is smaller than $\alpha(N) \times Ph_{Max} + \beta(N)$, the material is able to sustain more than N cycles with 50% probability of failure.

$$\sigma^{alt}_{eqvM} = \alpha(N) \times Ph_{Max} + \beta(N) \tag{1}$$

Consequently, for each of the profiles considered in this current study, the number of points where fatigue failure can occur for a number of cycles $N < 10^7$ with a risk of 10^{-3} are counted based on a manipulation of the Crossland method. To determine the precise values of N, this number of cycles to failure

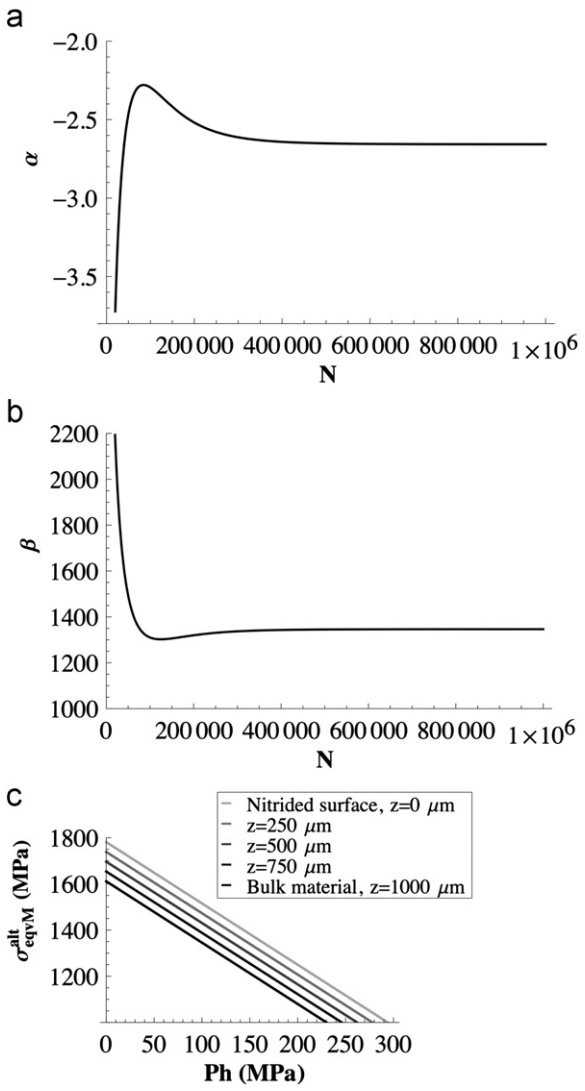

Fig. 7. Crossland parameters versus numbers of cycles to failure for quenched and tempered material, respectively, α(N) in 7(a) and β(N) in 7(b). In 7(c), changes in Crossland line.

must belong the specific domain restricted to 2×10^4 to 10^7. This is the domain of the experimental data, in terms of number of cycles to failure, that is used to define the fitted Wöhler fatigues curves. The 50% risk of failure associated with the Crossland line fitted to these curves is too large to give a useful parameter comparison. In order to reduce the failure risk to 10^{-3} for at N cycles, a shift that reduces the Crossland domain was implemented taking into account the assumption of a normal distribution of the experimental fatigue results and the known value of standard deviation on the fitting process. This method was summarised in [32] and is fully described in [42]. These results take into account all the points regardless of the predicted number N of cycles to rupture, for points with $2 \times 10^4 < N \leq 10^7$ cycles. The points with $\sigma_{eqvM} > \sigma_y$ were discarded from this assessment.

For the nitrided material, as shown in Fig. 7(c), $\alpha(N)$ is assumed to be constant in the nitrided layer in accordance with experimental results obtained with and without treatment [42]. These experimental results also show that $\beta(N)$ changes significantly with depth for nitrided material in comparison with material without nitriding. In the current study, these changes with depth were assumed to be linear from the top of the surface to the bulk material [42]. If the nitrided layer has depth d_n and the $\beta(N)$ coefficient has values $\beta_0(N)$ at the surface and $\beta_{d_n}(N)$ at depth d_n respectively, $\beta_d(N)$, the value of $\beta(N)$ at depth d is given by Eq. (2).

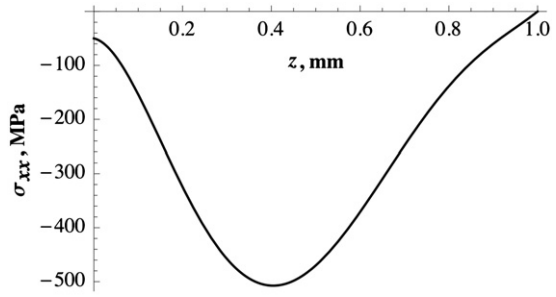

Fig. 8. Residual stress induced by nitriding as a function of depth.

$$\beta_d(N) = \left(1 - \frac{d}{d_n}\right) \times \beta_0(N) + \frac{d}{d_n} \times \beta_{d_n}(N) \quad (2)$$

In the case of nitriding, the mechanical loading is a superposition of the applied surface loading, given by the EHL calculations and the residual stress loading induced by the material treatment. For each point beneath the surface, the residual stresses were added to the normal load induced by EHL in accordance with the hypothesis of superposition. The residual stress component σ_{zz} was assumed to be equal to zero and components σ_{xx} and σ_{yy} were assumed to be compressive in the lateral and transverse directions with $\sigma_{xx}=\sigma_{yy}$. As shown in Fig. 8, the changes of these components in depth are given by a polynomial fitted curve with input data obtained using X-ray diffraction facilities [22]. Residual stress profiles induced by gaseous nitriding are dependant on the duration of the treatment [21]. Larger duration of treatment induces a shift in depth for the minimal stress.

3. Results and discussion

Results are analysed from two different points of view. The first analysis is concerned with the results obtained in the case of a rough pinion tooth meshing with a rough wheel tooth (R/R). In addition to a comparison of the results obtained on this current study of the contact between the rough on rough surfaces (R/R) a comparison with those obtained in a previous study [32] for the contact between a rough and a smooth surface (R/S) completes this analysis. The second analysis deals with the influence of nitriding treatment on the main significant parameters of the profile in the case of rough on rough meshing surfaces without nitriding (R/R) and with nitriding (R/R N).

3.1. Results on rough/rough profiles (R/R) without nitriding

The first analysis deals with the trends caused by variation of each parameter in the case of rough/rough profiles meshing. This is in order to detect the main mechanical influence of parameters using the three mechanical criteria described in Sections 2.3.3 and 2.3.4.

3.1.1. Maximal value of σ_{eqvM} analysis

Results of the maximum value of σ_{eqvM}, in time and in position of from 100 μm to 200 μm beneath the surface, obtained in the case of contact of two rough surfaces are shown in Fig. 9. This value is denoted $\sigma_{eqvM,max}$. The same scale is used for the seven graphs to clarify the main trends, and trends are discussed below in terms of the effects caused by increase of the parameter values. It can be seen, in Fig. 9(a), that HP, the land height of the carrier, is the most influential parameter. A strong increase is induced by this parameter. In Fig. 9(c), the same effect can be observed for

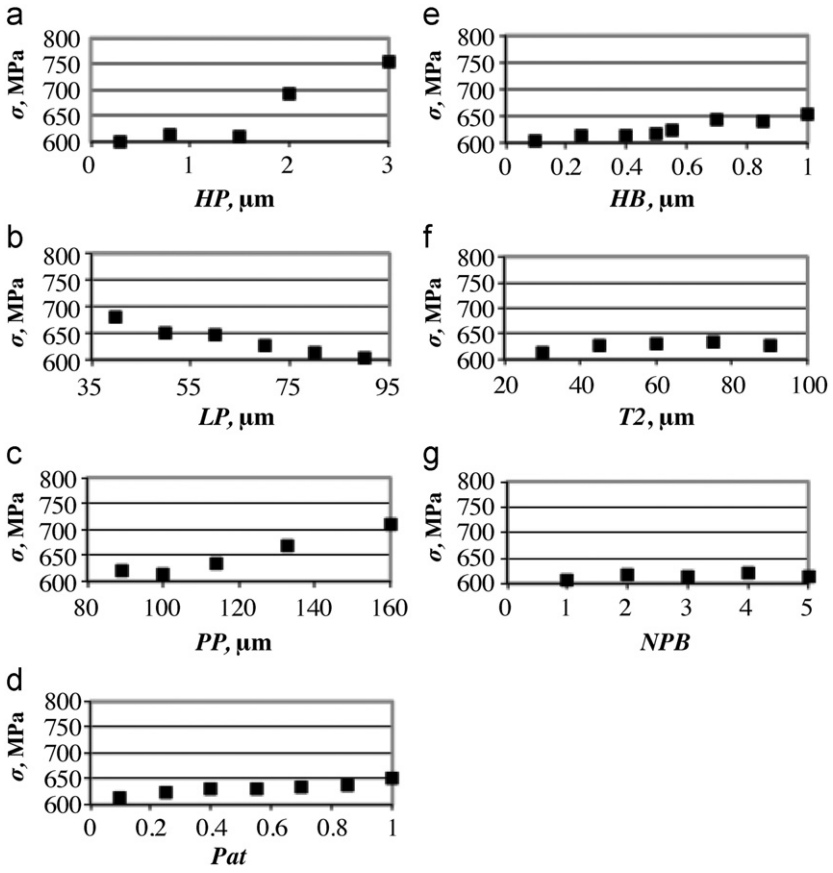

Fig. 9. Changes in the value of $\sigma = \sigma_{eqvM,max}$ for parameter variation of the rough profiles.

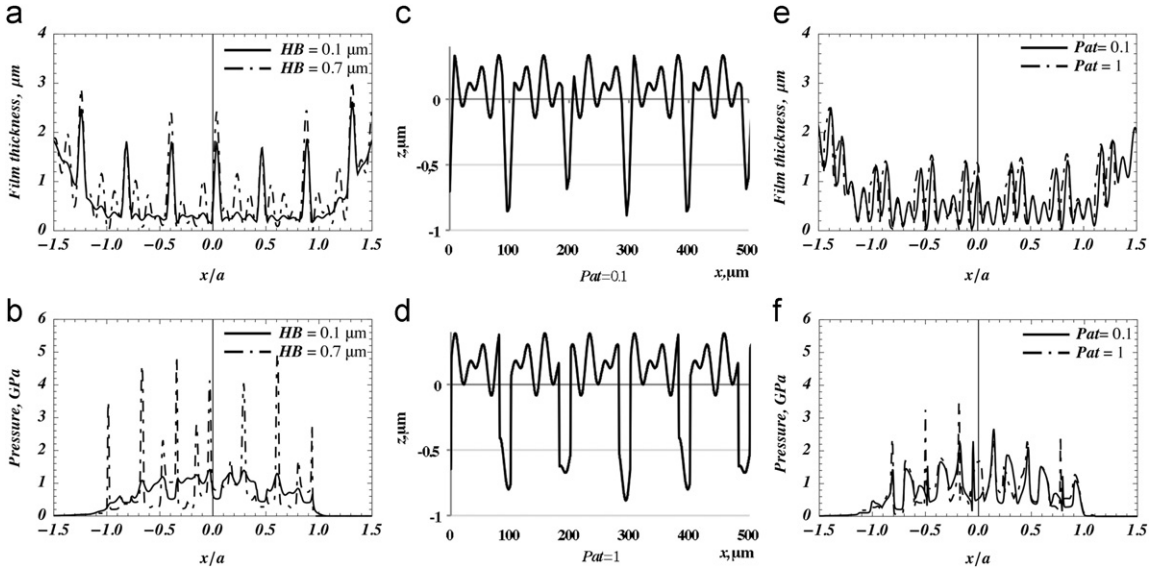

Fig. 10. Example timestep results from the EHL analysis for corresponding R/R cases for two different HB values (a) Film thickness, (b) Pressure. Figures (e) and (f) give corresponding results for Pat values of 0.1 and 1.0 with the resulting profiles illustrated in Figures (c) and (d).

the PP, the period of the carrier, with a smaller trend. In Fig. 9(b), LP, the land length of the carrier, induces a decrease in the stress. In Fig. 9(d), Pat, the engagement slope, and, in Fig. 9(e), HB, the height of the noise, generate an increase in the stress value but with a smaller effect over the parameter range considered. With these results, it is observed that roughness parameters T2 and NPB, respectively in Figs. 9(f) and (g), have little influence on the value of the $\sigma_{eqvM,max}$.

The changes can be explained by differences in terms of the surface boundary conditions. Coupling of two phenomena influences these conditions and these effects can be seen in the single timestep EHL results for R/R contacts given in Fig. 10. The first is due to the EHL response as the film thickness and pressure distribution changes in response to the geometry changes. It is logical that HP and HB, the heights of the carrier and noise cause changes to the pressure distributions. Figs. 10(a) and (b) gives the

film thickness and pressure response for different values of HB and shows that the pressure is greatly influenced by this parameter. The other significant effect is of change in loading intensity. Parameter Pat, the engagement and exit slope, causes an increase in the volume of the deep valley features as it is increased, as shown in Figs. 10(c) and (d). The effect on the film thickness and pressure are shown in Figs. 10(e) and (f).

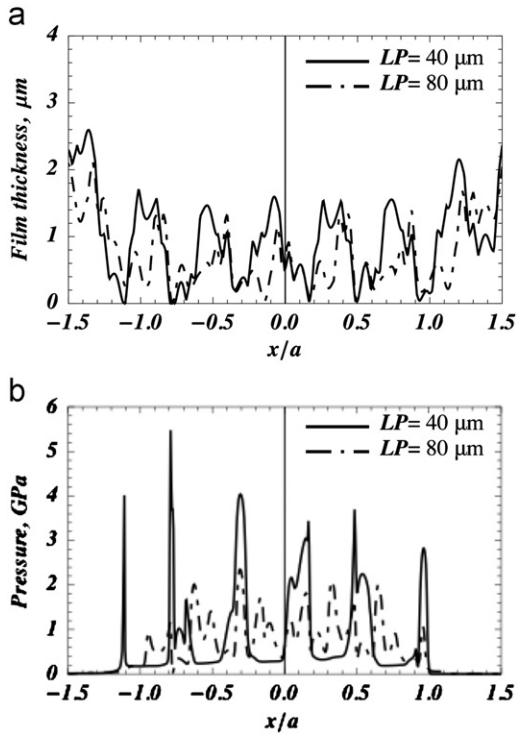

Fig. 11. Example timestep results from the EHL analysis for corresponding R/R cases for different LP values (a) Film thickness, (b) Pressure.

LP, the land length and PP, the period of the carrier are two parameters that influence the load distribution as they are directly linked with the bearing area of the surface. The effect of changes in LP can be observed in the single timestep results shown in Fig. 11. The boundary loading conditions strongly influence the value of $\sigma_{eqvM,max}$ and they are influenced by these parameters. Some changes in the location of $\sigma_{eqvM,max}$ were observed for the different profiles. These positions were found to be between 110 and 170 μm beneath the surface. For some parameter cases values of σ_{eqvM} close to the recorded $\sigma_{eqvM,max}$ value occurred at different depth positions so that the location of the maximum value was not necessarily unique within the 100–170 μm depth range.

3.1.2. Analysis of points with stress exceeding the yield point

Results for the number of points with $\sigma_{eqvM} > \sigma_y$ for variation of each of the seven parameters are shown in Fig. 12. The ordinate values are the ratio of the number of points with $\sigma_{eqvM} > \sigma_y$ to the total number of points. The total number of points is taken with the same discretisation for all the cases of calculation. In the zone of analysis, discretisation steps are taken equal to 10 μm for the width and to 1 μm in the depth.

The largest increase observed is due to PP, the period of the carrier in the Fig. 12(b). In Fig. 12(e), HB, the height of the noise also causes a significant increase. In Fig. 12(b), increasing the land length, LP, generates a decrease of the numbers of points with $\sigma_{eqvM} > \sigma_y$ and this change is of the order of that seen for

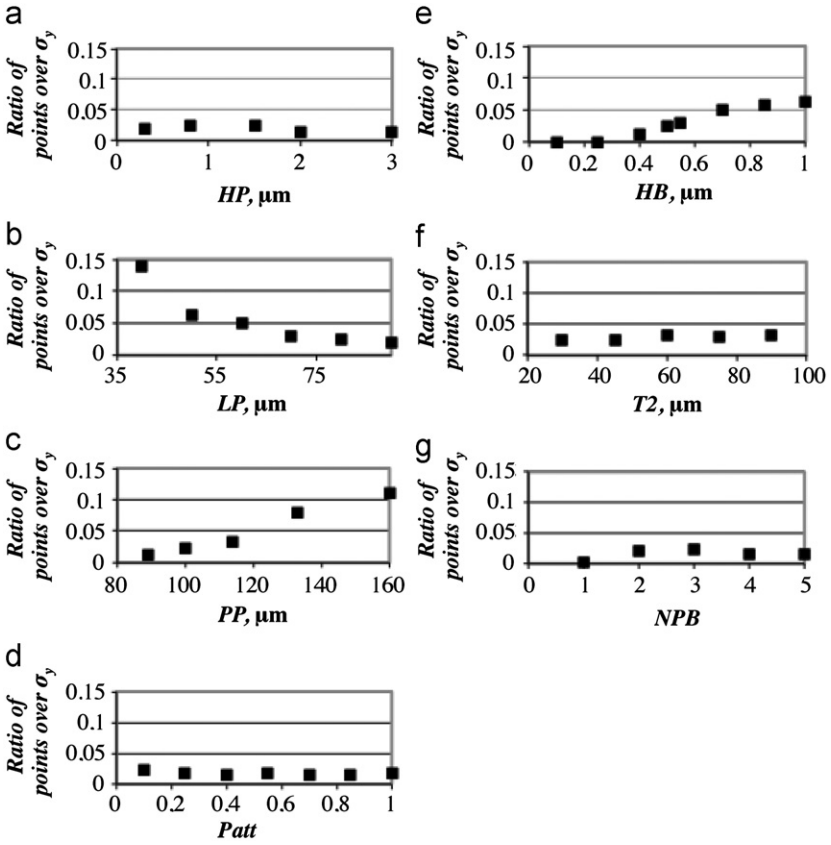

Fig. 12. Changes in ratio of points with $\sigma_{eqvM} > \sigma_y$ for parameter variation of the rough profiles.

parameter PP, in Fig. 12(d). No significant changes can be observed in the number of points due to changes in the others parameters.

The most significant effects observed are those due to changes in PP and LP, the period and land length of the carrier. Their influences are logical as the ratio of these two parameters gives the bearing ratio of the surface. The bearing ratio increases with an increase in the value of LP, and decreases with an increase in the value of PP. When the surface bearing ratio is larger, this results in lower surface stresses, and consequently smaller σ_{eqvM} for the points beneath the surface.

The influence of the height of the noise, HB, can be explained by considering the ratio of the height amplitude to the period. According to the literature [12,13], the bearing surface can be characterised by this ratio for a sinusoidal surface.

3.1.3. Fatigue analysis

In Fig. 13, the failure ratio is equal to the number of points to failure divided by the total number of points. In these last cases, the points considered are only those with $\sigma_{eqvM} < \sigma_y$. The total number of points is taken with the same discretisation for all the cases of calculation, and the points with $\sigma_{eqvM} > \sigma_y$ were discarded from this assessment. In the zone of analysis, discretisation steps are taken equal to 10 μm for the width and to 1 μm in the depth.

LP, the land length of the carrier appears in Fig. 13(b) to be the main parameter influencing the number of points. This effect can be described as a non-linear decay curve. The number of points experiencing failure increases almost linearly when PP, the period of the carrier, in Fig. 13(c) and HB, the height of the noise increase in Fig. 13(e). In this case again, the main parameters influencing fatigue appear to be those related to the bearing ratio of the surface. The dependence on HB shows that no points or only very few points, experience fatigue until the value of HB is greater than 0.4 μm. This change in behaviour maybe explained by a scale effect and the interaction of the two height parameters HB and HP as 0.4 μm is the half the value of the fixed value of HP, which was equal to 0.8 μm for the range of HB values, considered.

3.1.4. Comparison between rough/rough and rough/smooth contact results

The current results were compared with those obtained previously [32] for the case of rough on smooth surface contacts using the same roughness profile parameters and similar operating conditions. Overall, the influence of all pertinent parameters detected in the case of rough on smooth surfaces was confirmed in the case of rough on rough surfaces meshing. Only three differences are detected between these two different conditions of contact. For the rough on rough case, the engagement and exit slope of the carrier Pat, was found to be influential on the value of $\sigma_{eqvM,max}$. It was found that an increase of the number of yielding points is induced by an increase of the height of the noise HB. Only the height of the carrier HP, was found not to be a relevant parameter for the fatigue analysis.

3.2. Results for rough on rough surfaces with and without nitriding

With the previous results for the R/R case, the main significant parameters were LP, PP, and HB, the land length, the period of the carrier and the height of noise, respectively. The analysis of the nitriding effect was conducted by considering the results for these three parameters with and without including the effect of

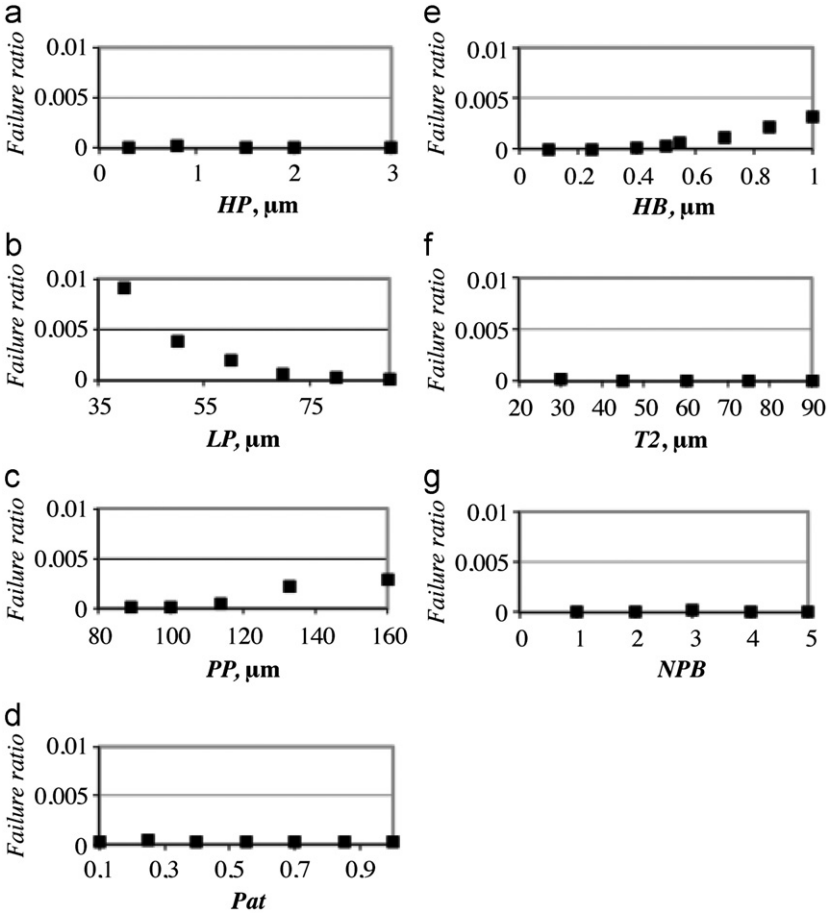

Fig. 13. Change in the ratio of points to failure for parameter variation of the rough profiles.

nitriding on yield strength and residual stress. Since the elastic modulus is assumed to be unaltered by the nitriding process the EHL pressure distributions remain the same and there is no change in $\sigma_{eqvM,max}$. The investigation was therefore based on the number of points with $\sigma_{eqvM} > \sigma_y$, and the number of points experiencing calculated fatigue failure.

3.2.1. Analysis of points with stress exceeding the yield point

Fig. 14 shows the results for the ratio of points with $\sigma_{eqvM} > \sigma_y$ for the two cases with the nitrided results shown in the left hand figures. Note that as the effect of nitriding is significant the ordinate scales are different for the two cases.

The nitriding benefits can be observed with the significant reduction of the number of points with $\sigma_{eqvM} > \sigma_y$. The trend apparent for each parameter is unchanged by nitriding but the highest number of points identified is reduced by a factor of between 14 and 30 according to the parameter considered.

3.2.2. Fatigue analysis

In Fig. 15, the results for the ratio of points experiencing calculated fatigue failure are compared for the two cases. Again nitriding causes a significant reduction in the number of points counted and the ordinate scales are different to facilitate comparison of trends. The same trends are observed for each parameter with and without nitriding with the maximum failure ratio value reduced by a factor of about 3 when nitriding is included. In Figs. 15(a) and (d), a marked decrease of the number of points to failure is shown when LP, the land length increases. Increased values of both PP, the period of the carrier, in Figs. 15(b) and (e), and HB, the height of the noise, in Figs. 15(c) and (f), cause increased numbers of points experiencing fatigue.

3.3. Summary of results

It was found that five of the profile parameters have a significant influence on the pitting effect in terms of their effect on changes of the maximal equivalent von Mises stress developed in the contacting material. The most significant parameters were the height, HP, the period, PP, and the land length, LP, of the carrier component of the roughness profile.

In terms of the capability of the material to sustain the mechanical loadings the effects of the seven parameters of the rough profile were analysed to determine the numbers of points subject to yielding at a specified yield stress of 1 GPa for the basis material. It was found that two carrier parameters; the land length LP, and the period PP, and one noise parameter, the noise height HB, induce significant changes in the number of yielding points.

A fatigue analysis was carried out using the Crossland criterion with the material properties of the basis material. Again the three parameters LP, PP and HB were found to have the greatest effect on the level of fatigue experienced by the material in these calculations.

Table 6 shows that most of the parameters determined to be influential are from the carrier component of the rough profile. This can be explained by the fact that LP and PP (the land length and the period of the carrier) influence directly the bearing area in the contact zone. For the noise, only the height HB, is demonstrated as playing a role in the changes of $\sigma_{eqvM,max}$, the number of points with $\sigma_{eqvM} > \sigma_y$ and the number of points to failure. This can be explained because this parameter is very influential in determining the local variation in lubricant pressure and EHL film thickness.

To complete this current study, an analysis of the effect of nitriding on the material was investigated for the main pertinent parameters for fatigue. Taking into account the material changes and residual stresses induced by the nitriding process, calculations

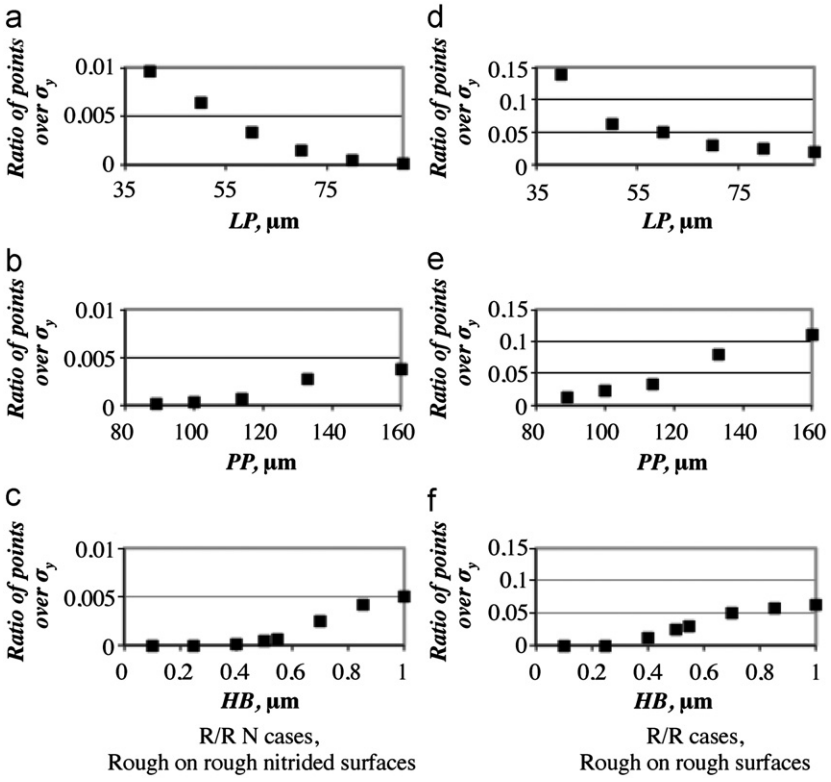

Fig. 14. Results for the ratio of points with $\sigma_{eqvM} > \sigma_y$ for the nitrided steel on the left, and for the basis steel on the right.

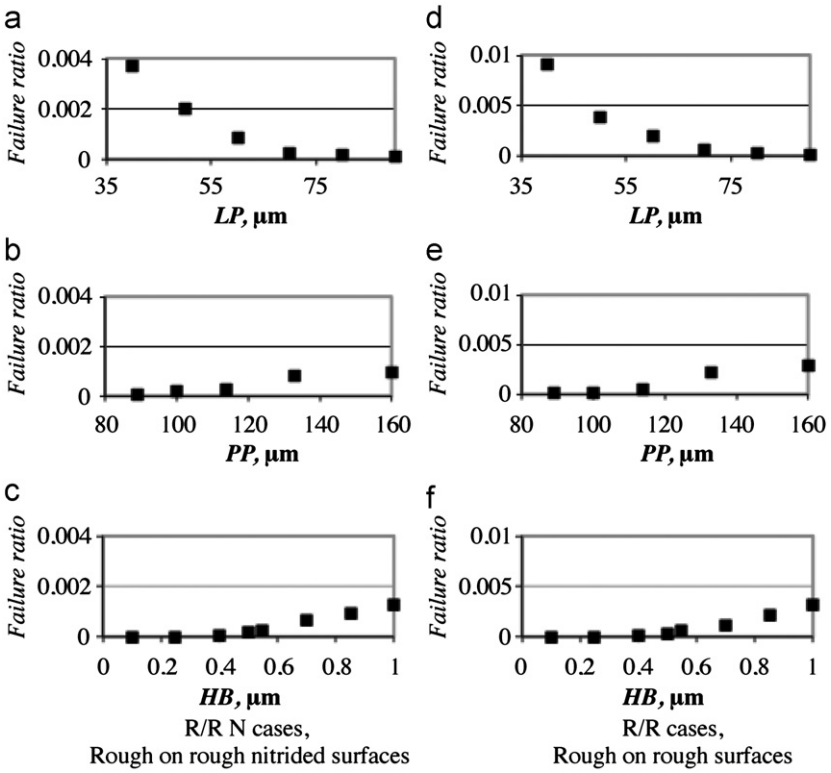

Fig. 15. Results for the ratio of points experiencing fatigue failure for the nitrided steel on the left, and for the basis steel on the right.

Table 6
Summarising the main parameters influencing the maximum equivalent von Mises stress, the extent of material yield, and the extent of calculated fatigue and their effect in terms of increasing parameter values.

Parameter	$\sigma_{eqvM,max}$		Number of points with $\sigma_{eqvM} > \sigma_y$		Numbers of points subject to fatigue	
	Trend	Influence	Trend	Influence	Trend	Influence
HP, land height	Increase	Strong	No relevant		Not relevant	
LP, land length	Decrease	Strong	Decrease	Strong	Decrease	Strong
PP, cycle of carrier	Increase	Strong	Increase	Strong	Increase	Average
Pat, exit or engagement slope	Increase	Weak	Not relevant		Not relevant	
HB, height of noise	Increase	Weak	Increase	Average	Increase	Average

show the same trend effects for the land length LP, and the period of the carrier PP. The height of the noise HB, is confirmed as a pertinent parameter. The number of points experiencing yield was reduced by at least an order of magnitude as a result of the increased yield strength in the nitrided layer. A large reduction of the number of points experiencing fatigue failure was also observed, in agreement with the experimental knowledge of the benefit of nitriding.

4. Conclusion

In conclusion, an investigation was conducted to find the most relevant parameters in roughness profiles that can be used to control surface damage in the form of micropitting of and involute steel gear pair. The originality of this approach was to build generic roughness profiles with only seven parameters taking in account the specific morphology of the ground and superfinished surfaces of rough gear teeth. In the study, EHL code was used to define the surface loading for the case of contact between two rough surfaces. A semi-analytical method was used to calculate the sub-surface stress tensor history and it was found that the severity of the sub-surface loading is dependent on five of the roughness parameters specified. Three parameters play a major role controlling the number of points exceeding the elasticity limit, and the number experiencing fatigue in accordance with the Crossland fatigue criterion.

Acknowledgement

Dr Fabre's sabbatical period at the Cardiff School of Engineering allowed the research to be conducted. Thanks are due to the M2P department of Arts et Métiers ParisTech, to Arts et Métiers ParisTech—Aix en Provence, and to the MécaSurf laboratory for supporting the visit financially, and to Cardiff University for provision of research facilities. Dr Sharif's contribution to the research was supported financially by UK Engineering & Physical Sciences Research Council (EPSRC) with Grant no. EP/G06024X/1.

References

[1] Alban LE. Systematic analysis of gear failures. 4th ed.. USA: ASM; 1993.
[2] Höhn BR, Michaelis K. Influence of oil temperature on gear failure. Tribology International 2004;37:103–9.
[3] Snidle RW, Evans HP. Some aspects of gear tribology. Proceedings of the Institution of Mechanical Engineers, Part C: Journal of Mechanical Engineering Science 2009;223:103–41.

[4] Poëssel P, Gras R, Gaudin J. Lifetime prediction of helicopter gears: experimental investigations and computer modelling. In: Mianny D, Costa P, François D, Pineau A, editors. Advances in mechanical behaviour, plasticity and damage. oxford: Elsevier; 2000. p. 997–1002.
[5] Evans HP, Snidle R, Sharif KJ. Analysis of micro-elastohydrodynamic lubrication and surface fatigue in gear micropitting tests. In: Proceedings of the ASME 2011 International Design Engineering Technical Conferences & Computers and Information in Engineering Conference, IDETC/CIE 2011, Washington, DC, USA; 2011.
[6] Qiao H, Evans HP, Snidle RW. Comparison of fatigue model results for rough surface elastohydrodynamic lubrication. Proceedings of the Institution of Mechanical Engineers, Part J: Journal of Engineering Tribology 2008;222: 381–93.
[7] Cardoso NFR, Martins RC, Seabra JHO, Igartua A, Rodriguez JC, Luther R. Micropitting performance of nitrided steel gears lubricated with mineral and ester oils. Tribology International 2009;42:77–87.
[8] Lainé E, Olver AV, Beverdge TA. Effect of lubricants on micropitting and wear. Tribology International 2008;41:1049–55.
[9] Tasan YC, de Rooij MB, Schipper DJ. Changes in the micro-geometry of a rolling contact. Tribology International 2007;40:672–9.
[10] Akbarzadeh S, Khonsari MM. Experimental and theoretical investigation of running-in. Tribology International 2011;44:92–100.
[11] Boucly V, Nélias D, Green I. Modeling of the rolling and sliding contact between two asperities. Journal of tribology 2007;129:235–45.
[12] Paulin C, Ville F, Sainsot P, Coulon S, Lubrecht T. Effect of rough surfaces on rolling contact fatigue: Theoretical and experimental analysis. Elsevier tribology Series 2003;43:611–7.
[13] Labiau A, Ville F, Sainsot P, Querlioz E, Lubrecht T. Effect of sinusoidal surface roughness under starved conditions on rolling contact fatigue. Proceedings of the Institution of Mechanical Engineers, Part J: Journal of Engineering Tribology 2008;222:193–200.
[14] Crossland B. Effects of large hydrostatic pressures on the torsional fatigue strength of an alloy steel. In: Proceeding of the International Conference on Fatigue of metals, London: SEP; 1956, p. 138–149.
[15] Ligier JL. Lubrification des paliers de moteur. Paris: Technip; 1997.
[16] Standard NF EN ISO 4287; December 1998.
[17] Locquet JN, Barrallier L, Soto R, Charaï A. Complete TEM Investigation of Nitrided Layer for a Cr Alloy Steel. Microscopy Microanalysis Microstructures 1997;8:335–52.
[18] Jacq C, Lormand G, Nélias D, Girodin D, Vincent A. On the influence of residual stresses in determining the micro-yield stress profile in a nitrided steel by nano-indentation. Materials Science and Engineering A 2003;342:311–9.
[19] Jones BK, Martin JW. The effect of residual stresses on the fatigue failure of nitride En41B steel. Fracture 1977:1259–65 ICF4, Waterloo, Canada.
[20] Waterhouse RB. The formation, structure, and wear properties of certain non-metallic coatings of metal. Wear 1965;8:421–47.
[21] Jegou S, Barrallier L, Kubler R, Somers MAJ. Evolution of residual stress in diffusion zone of a model Fe-Cr-C alloy during nitriding. HTM Journal of Heat Treatment and Materials 2011;66(3):135–42.
[22] Locquet JN. Caractérisations métallurgiques et mécaniques de couches nitrurées. Relation microstructure-comportement. PHD Thesis ENSAM, Aix-en-Provence; 1998.
[23] Chaussumier M, Greco E, Desvignes M. Multiaxial fatigue of nitrurated material. In: Proceeding of Dimensionnement en fatigue des structures: démarche et outils, Paris: Société française de métallurgie et de matériaux; 1999, p. P3.1–P3.8.
[24] Fabre A, Barrallier L. Neutron determination of residual stress in a nitrided notched part. Materials Science Forum 2005;490-491:251–6.
[25] Goret V, Fabre A, Barrallier L, Vardon P. Evaluation by synchrotron radiation of shape factor effects on residual stress in nitrided layers. Mater. Science Forum 2006;524-525:285–90.
[26] Chang L, Zhao Y. Fundamental differences between Newtonian and non-Newtonian micro-EHL results. Transactions of the ASME, Journal of Tribology 1995;117:29–35.
[27] Hughes TG, Elcoate CD, Evans HP. Coupled solution of the elastohydrodynamic line contact problem using a differential deflection method. Proc IMechE, Part C:J. of Mech Engineering Science 2006;214:585–98.
[28] Elcoate CD, Evans HP, Hugues TG, Snidle RW. Transient elastohydrodynamic analysis of rough surfaces using a novel coupled differential deflection method. IMechE, PartJ:J. of Mechanical Engineering Tribology 2001;215: 319–37.
[29] Holmes MJA, Evans HP, Snidle RW. Contribution to a discussion on the paper "Elastohydrodynamic lubrication in extended paper ranges Part II: Load effect" by D. Zhu, Tribology Transactions 2003; 46: 282-283.
[30] Holmes MJA, Evans HP, Snidle RW. Analysis of mixed lubrication effects in simulated gear tooth contacts. Trans ASME Jn of Tribology 2005;127:61–9.
[31] Holmes MJA, Hughes TG, Evans HP, Snidle RW. Transient elastohydrodynamic point contact analysis using a new coupled differential deflection method: Part 2 Results. Proceedings of the Institution of Mechanical Engineers, Part J: Journal of Engineering Tribology 2003;217:305–21.
[32] Fabre A, Barrallier L, Desvignes M, Evans HP, Alanou MP. Microgeometrical influences on micropitting fatigue damage: multiscale analysis. Proceedings of the Institution of Mechanical Engineers, Part J: Journal of Engineering Tribology 2011;225:419–27.
[33] Fabre A, Barrallier L, Desvignes M, Evans HP, Alanou MP. Influence of roughness on the stress tensor: contact between a rough and smooth tooth in a spur gearing application. In: Zaïdi H, Rivière JP, Frêne J, editors. Lubrification et tribologie des revêtements minces, Poitiers: Presses Polytechniques et Universitaires Romandes; 2010. p. 167–76.
[34] Johnson KL. Contact Mechanics. Cambridge: Cambridge University Press; 1985.
[35] Lemaître J, Chaboche JL. Mécanique des matériaux solides. 2nd ed. Paris: Dunod; 2004.
[36] Dang-Van K, Cailletaud G, Flavenot JF, Douaron L, Lieurade HP. Criterion for high-cycle fatigue failure under multiaxial loading. In: Brown M, Miller K, editors. Biaxial and Multiaxial Fatigue. London: Mechanical Engineering Publications; 1989. p. 459–78.
[37] Palin Luc T. Fatigue sous chargements d'amplitude variable. In: Bathias C, Pineau A, editors. Fatigue des matériaux et des structures. Paris: Lavoisier; 2008. p. 205–48.
[38] Zenner H, Simbürger A, Liu J. On the fatigue limit of ductile metals under complex multiaxial loading. International Journal of Fatigue 2000;22(2): 137–45.
[39] Banvillet A, Lagoda L, Macha E, Nieslony A, Palin-Luc T, Vittori JF. Fatigue life under non-gaussian random loading from various models. International Journal of Fatigue 2004;26(4):349–63.
[40] Miner M. Cumulative damage in fatigue. J of applied mechanics Trans. ASME 1945;12:159–64.
[41] Palmgren A. Die Lebbensdauer vo kugellagern. VDI-Zeitschrift 1924;58: 339–41.
[42] Chaussumier M. Un modèle statistique de calculs en fatigue multiaxiale pour les pièces mécaniques en acier nitruré. PhD thesis. ENSAM, Aix-en-Provence; 1998.